Resource

Cell

High-Resolution Mapping Reveals a Conserved, Widespread, Dynamic mRNA Methylation Program in Yeast Meiosis

Schraga Schwartz,[1,8] Sudeep D. Agarwala,[2,8] Maxwell R. Mumbach,[1] Marko Jovanovic,[1] Philipp Mertins,[1] Alexander Shishkin,[1] Yuval Tabach,[3,4] Tarjei S. Mikkelsen,[1] Rahul Satija,[1] Gary Ruvkun,[3,4] Steven A. Carr,[1] Eric S. Lander,[1,5,6] Gerald R. Fink,[1,2,*] and Aviv Regev[1,7,8,*]

[1]Broad Institute of MIT and Harvard, Cambridge, MA 02142, USA
[2]Whitehead Institute for Biomedical Research, Cambridge, MA 02142, USA
[3]Department of Molecular Biology, Massachusetts General Hospital, Boston, MA 02114, USA
[4]Department of Genetics, Harvard Medical School, Boston, MA 02115, USA
[5]Department of Biology, Massachusetts Institute of Technology, Cambridge, MA 02139, USA
[6]Department of Systems Biology, Harvard Medical School, Boston, MA 02114, USA
[7]Department of Biology, Howard Hughes Medical Institute, Massachusetts Institute of Technology, Cambridge, MA 02139, USA
[8]These authors contributed equally to this work
*Correspondence: gfink@wi.mit.edu (G.R.F.), aregev@broadinstitute.org (A.R.)
http://dx.doi.org/10.1016/j.cell.2013.10.047

SUMMARY

N^6-methyladenosine (m^6A) is the most ubiquitous mRNA base modification, but little is known about its precise location, temporal dynamics, and regulation. Here, we generated genomic maps of m^6A sites in meiotic yeast transcripts at nearly single-nucleotide resolution, identifying 1,308 putatively methylated sites within 1,183 transcripts. We validated eight out of eight methylation sites in different genes with direct genetic analysis, demonstrated that methylated sites are significantly conserved in a related species, and built a model that predicts methylated sites directly from sequence. Sites vary in their methylation profiles along a dense meiotic time course and are regulated both locally, via predictable methylatability of each site, and globally, through the core meiotic circuitry. The methyltransferase complex components localize to the yeast nucleolus, and this localization is essential for mRNA methylation. Our data illuminate a conserved, dynamically regulated methylation program in yeast meiosis and provide an important resource for studying the function of this epitranscriptomic modification.

INTRODUCTION

DNA, RNA, and proteins are all covalently modified postsynthesis, potentially impacting their function. Although DNA and protein modifications have been extensively studied, our understanding of mRNA modifications is limited. The methylation of adenosine at the N^6 position to form N^6-methyladenosine (m^6A) is among the most abundant base modifications known in eukaryotic mRNA (Desrosiers et al., 1975). Orthologs of the RNA-based N^6-adenosyl methyltransferases (MTases) that catalyze this modification are present in almost all eukaryotes, and their depletion or disruption causes lethality in metazoans (Bokar, 2005; Dominissini et al., 2012; Hongay and Orr-Weaver, 2011) and severe developmental defects in plants (Zhong et al., 2008). Interestingly, the FTO protein, which is genetically associated with human obesity, acts as a specific m^6A demethylase (Jia et al., 2011).

Significant technical and experimental limitations have hindered the study of m^6A modifications. First, because m^6A neither changes the base-pairing properties nor inhibits reverse transcription, identification of modified transcripts has depended on immunoprecipitation using antibodies against m^6A (Bodi et al., 2010; Bringmann and Lührmann, 1987; Dominissini et al., 2012; Meyer et al., 2012). Recent transcriptome-wide mappings, termed m^6A-seq (Dominissini et al., 2013) or MeRIP-Seq (Meyer et al., 2012), have revealed that m^6A accumulates near stop codons and atypically long exons and that methylation sites in mammals are associated with an RRACT (R = A/G) consensus sequence, consistent with earlier studies (Dimock and Stoltzfus, 1977; Schibler et al., 1977; Wei et al., 1976). However, the resolution of these maps was only ~24 nt around the methylation site, as estimated from the median distance from an identified peak to the closest consensus sequence (Dominissini et al., 2012). Thus, to date, only a single methylated site has been mapped at single-nucleotide resolution on eukaryotic mRNA (Horowitz et al., 1984; Narayan and Rottman, 1988). Second, experimental depletion of the methylation complex in mammals results in apoptosis (Bokar, 2005; Dominissini et al., 2012; Hongay and Orr-Weaver, 2011), rendering it difficult to dissect the functional role of methylation. Third, the mammalian methylation landscape appears to be mostly static across cell types, tissues, and stimuli (Dominissini et al., 2012; Meyer et al., 2012), limiting our ability to elucidate how methylations emerge.

By contrast, mRNA methylation in the yeast *Saccharomyces cerevisiae* occurs only during meiosis (Agarwala et al., 2012;

Clancy et al., 2002; Hongay et al., 2006; Shah and Clancy, 1992), providing a unique opportunity to dissect its dynamics and regulation. Genetic screens in yeast have identified a core RNA methyltransferase (MIS) complex comprised of Ime4 (orthologous to mammalian methyltransferase like 3 [METTL3]), Mum2 (orthologous to mammalian Wilm's-tumor-1-associated protein [WTAP]), and a third ancillary factor, Slz1 (Agarwala et al., 2012). The MIS complex is induced during meiosis, and defects that abrogate its mRNA methylation activity delay meiotic entry (Agarwala et al., 2012; Clancy et al., 2002; Hongay et al., 2006; Shah and Clancy, 1992). Elimination of MIS components in yeast is not lethal (Agarwala et al., 2012; Clancy et al., 2002; Hongay et al., 2006; Shah and Clancy, 1992), allowing experimental exploitation of such strains.

Here, we used a high-resolution assay coupled with mutants defective in methylation to identify m^6A sites at nearly single-base resolution in meiotic yeast transcripts. Our approach allows us to dissect *cis* and *trans* elements governing methylation onset and offset and provides a broad overview on a conserved and dynamically regulated methylation program in yeast meiosis and an important resource toward addressing its function.

RESULTS

m^6A-Seq Defines the MIS-Dependent Yeast Methylome

To map m6A sites in yeast, we used a highly optimized m6A-seq approach (Figure S1A available online). Previously published protocols (1) required substantial input material, (2) had relatively low resolution around the actual methylated site, and (3) did not provide a way to directly assess false positives (Dominissini et al., 2012; Meyer et al., 2012). We optimized the protocol (Experimental Procedures) to decrease the required mRNA starting material (from 400 μg $polyA^+$ mRNA to 5 μg), increase resolution (by decreasing fragment size and employing a ligation-based strand-specific library preparation protocol capturing both ends of the fragmented RNA, ensuring that the methylated position is within the sequenced fragment), and increase scale. Finally, to determine false positives, we used a negative control of strains with *ime4*Δ/Δ, which do not accumulate m^6A.

We applied m^6A-seq to (1) mRNA isolated from an *ndt80*Δ/Δ strain undergoing meiosis, which arrests during meiotic G2/prophase when bulk m^6A-mRNA levels are at their peak (Agarwala et al., 2012), and (2) as a negative control, an *ime4*Δ/Δ strain, which arrests at the same time point as the *ndt80*Δ/Δ strain but does not accumulate m^6A (Agarwala et al., 2012; Clancy et al., 2002). We aligned reads from immunoprecipitated (IP) and input samples to the SK1 reference genome and called peaks based on presence in the IP samples and absence in the input (Experimental Procedures).

Of the 3,294 sites present in at least two of three *ndt80*Δ/Δ biological replicates, 1,664 (50.5%) were absent from both the input samples (Experimental Procedures) and the *ime4*Δ/Δ samples, suggesting that these are true methylated sites ("MIS dependent"; Figure 1A). The remaining peaks were "MIS independent": present in both wild-type and *ime4*Δ/Δ experiments, but not in the input samples. To confirm that these MIS-independent sites were experimental artifacts, we applied m^6A-seq to nonmethylated RNA from 17 in-vitro-transcribed genes with MIS-independent peaks. In 13 of 17 cases, we obtained peaks in precisely the same regions as in the yeast samples (Figure S1B). These false-positive sites were enriched in degenerate purine-rich sequence motifs (Figure S1C), suggesting that the antibody may be biased toward such sequences. The *ime4*Δ/Δ strain allows us to remove these false-positive sites. In all subsequent analyses, we only considered a conservative, high-quality, yeast mRNA methylome of 1,308 putative m^6A sites within 1,183 genes detected only in the presence of *IME4* (Experimental Procedures and Table S1).

We further validated that the yeast mRNA methylome defines targets for MIS-mediated methylation. First, m^6A-seq of cells either encoding a catalytically defective allele of *IME4* background (*ime4-cat*) or a deletion of *MUM2* leads to loss of enrichment, specifically at the MIS-dependent sites (Figure 1A), showing that MIS complex function is necessary for site methylation. Second, m^6A-seq of cells growing under vegetative conditions but overexpressing the three components of the MIS complex (Agarwala et al., 2012) yields profiles very similar to those obtained in meiosis, suggesting that induction of the three components of the MIS complex is sufficient to faithfully recapitulate the meiotic mRNA methylation program (Figures 1A and 1B).

Function of Methylated Genes

The 1,183 methylated genes span diverse functions and are enriched in functions highly relevant to meiosis, including DNA replication ($p = 1.8 \times 10^{-6}$), mismatch repair ($p = 1.3 \times 10^{-4}$), and synaptonemal complex formation ($p = 1.5 \times 10^{-3}$), even when using an expression-matched gene set as background (data not shown). In particular, 105 of 376 curated meiosis-specific genes are methylated (Table S1 and Extended Experimental Procedures). Other methylated transcripts span a wide set of functions, including signaling, maintenance, and metabolism, though we cannot preclude their meiosis-specific role. Notably, we did not observe m^6A in the *IME1* and *IME4* transcripts (Bodi et al., 2010) and found a methylated region in the *IME2* transcript different from that previously described (Bodi et al., 2010) (Figure S1D).

m^6A Occurs in a Consensus Motif that Is Necessary for Methylation

The overwhelming majority of motifs enriched within a 50 bp window centered around m^6A-peaks harbored an RGAC (R = A/G) consensus sequence (Figures 1C and 1D and Experimental Procedures), reminiscent of yet distinct from the RRACU consensus motif around mammalian m^6A sites (Dimock and Stoltzfus, 1977; Dominissini et al., 2012; Meyer et al., 2012; Schibler et al., 1977; Wei et al., 1976). Reflecting nearly single-nucleotide resolution, the median distance between the enriched peak and the nearest RGAC consensus site is 3 nt (57 nt in an equally sized randomly selected control set; Mann-Whitney, $p = 6.9 \times 10^{-215}$; Figure 1D). Notably, before filtering the MIS-independent peaks, this median distance is ~18 nt (Figure 1D), similar to that previously reported in mammals (Dominissini et al., 2012; Meyer et al., 2012).

To validate the consensus, we selected eight peaks in distinct genes and generated diploid strains carrying single point mutations that eliminate the methylation consensus sequence. We mutated either the methylated adenosine or one of its two flanking positions without altering the protein sequence. In all eight

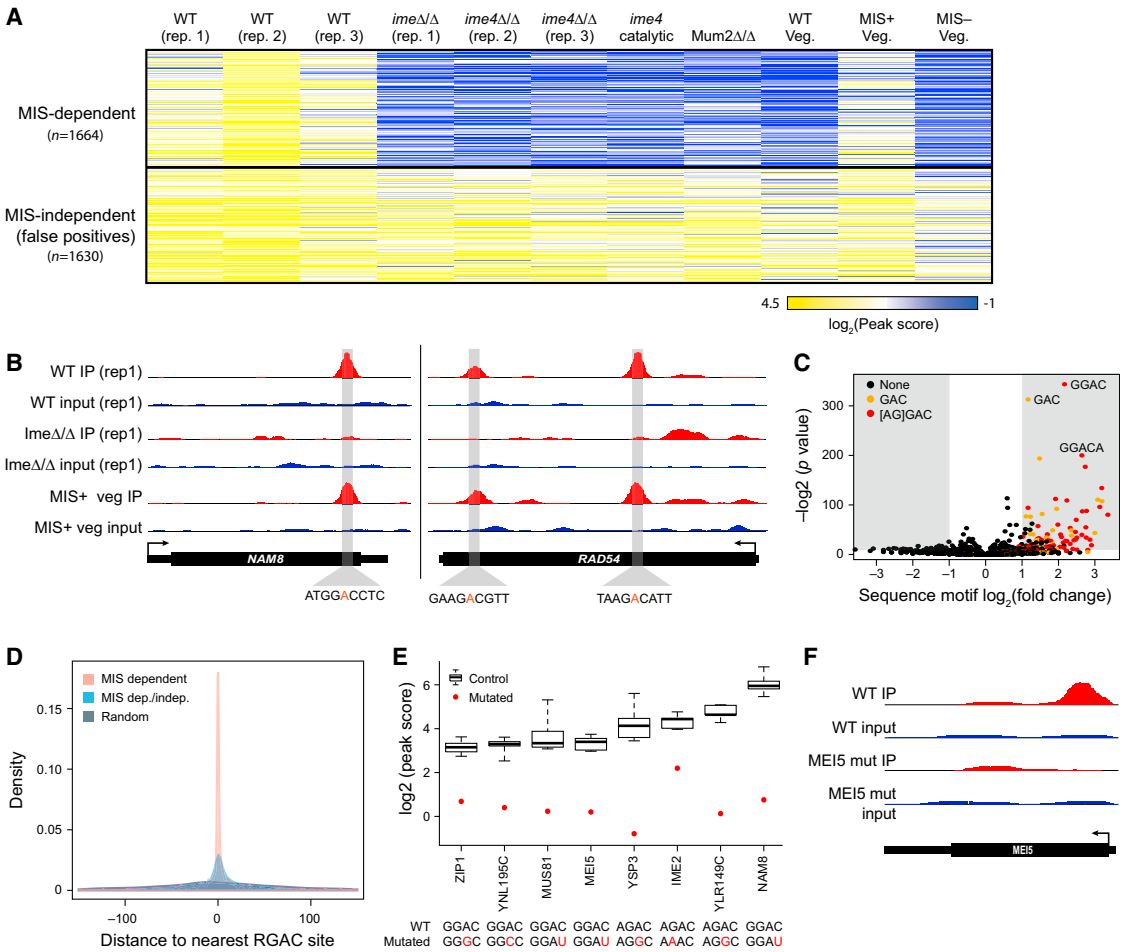

Figure 1. Genome-wide Identification of MIS-Dependent m^{6}A Sites with m^{6}A-Seq

(A) Methylation profiles. Heatmap shows the $\log_2$-transformed peak scores (fold change of enrichment of a site over the median level of the gene; yellow, high; blue, low) for 3,294 peaks (rows) that were enriched in at least two of the three WT (*ndt80*Δ/Δ, SAy841) replicates across different conditions and perturbations (columns; *ime4*Δ/Δ *ndt80*Δ/Δ, SAy996; *ime4*-cat *ndt80*Δ/Δ, SAy1280; *mum2*Δ/Δ, SAy1310; wild-type, SAy821; MIS induction, SAy1248). Sites are clustered using k-means clustering. MIS-dependent and -independent sites are marked on top and bottom, respectively.

(B) Example methylated loci. Sequence coverage from m^{6}A-Seq (IP) and control (input) experiments in different strains (tracks) for *NAM8* (left) and *RAD54* (right). (Gray highlight) A 50 nt region surrounding the called peak position, with putative methylation consensus sequence (bottom).

(C) Volcano plot of the enrichment (y axis) and fold change (x axis) of all 3–6 nt k-mers in a 50 nt window surrounding identified methylation sites, compared to randomly selected regions from the same genes. (Shaded regions) Statistically depleted (left) or enriched (right) regions (fold change > 2; Bonferroni-corrected p values < 0.05). (Orange) Sites comprising the GAC core motif; (red) sites comprising a full RGAC motif.

(D) Methylated sites at near single-nucleotide resolution. Density plots of the distribution of the distance between the identified peak and the most adjacent RGAC motif (x axis) for the 1,308 MIS-dependent peaks (red), all MIS-dependent and -independent sites (blue), and randomly selected sites within the same genes as the MIS-dependent peaks (gray).

(E and F) Sequence motif is essential for methylation.

(E) m^{6}A-seq peak scores (y axis) for eight genes measured in strains in which the methylated sequence motif was either WT (top sequence) or mutated (bottom sequence, mutation in red). The distribution of peak scores along WT strains (n = 9) is indicated with box plots (error bars, min and max). (Red dot) Mutant peak score.

(F) m6A-Seq (IP) and control (input) for the WT (two top tracks) and mutant (two bottom tracks) alleles of MEI5.

See also Figure S1 and Table S1.

cases, the peaks were eliminated in the mutated strains (Figures 1E and 1F) to the same effect when the mutation was in the methylated adenosine or in positions +1 or −1, suggesting that all three positions are required for methylation. In none of the eight cases did we observe compensatory methylation of adjacent noncanonical positions, as was previously reported in an in vitro point-mutation study (Narayan et al., 1994).

Methylation Sites Can Be Predicted from Sequence and Structural Features

We next leveraged the enhanced resolution and quality of our assay to examine which sequence and structural features are associated with bona fide methylated sites. First, we determined a broader sequence motif from a conservatively selected subset of 711 sites in which the peak was within 5 nt of an RGAC site.

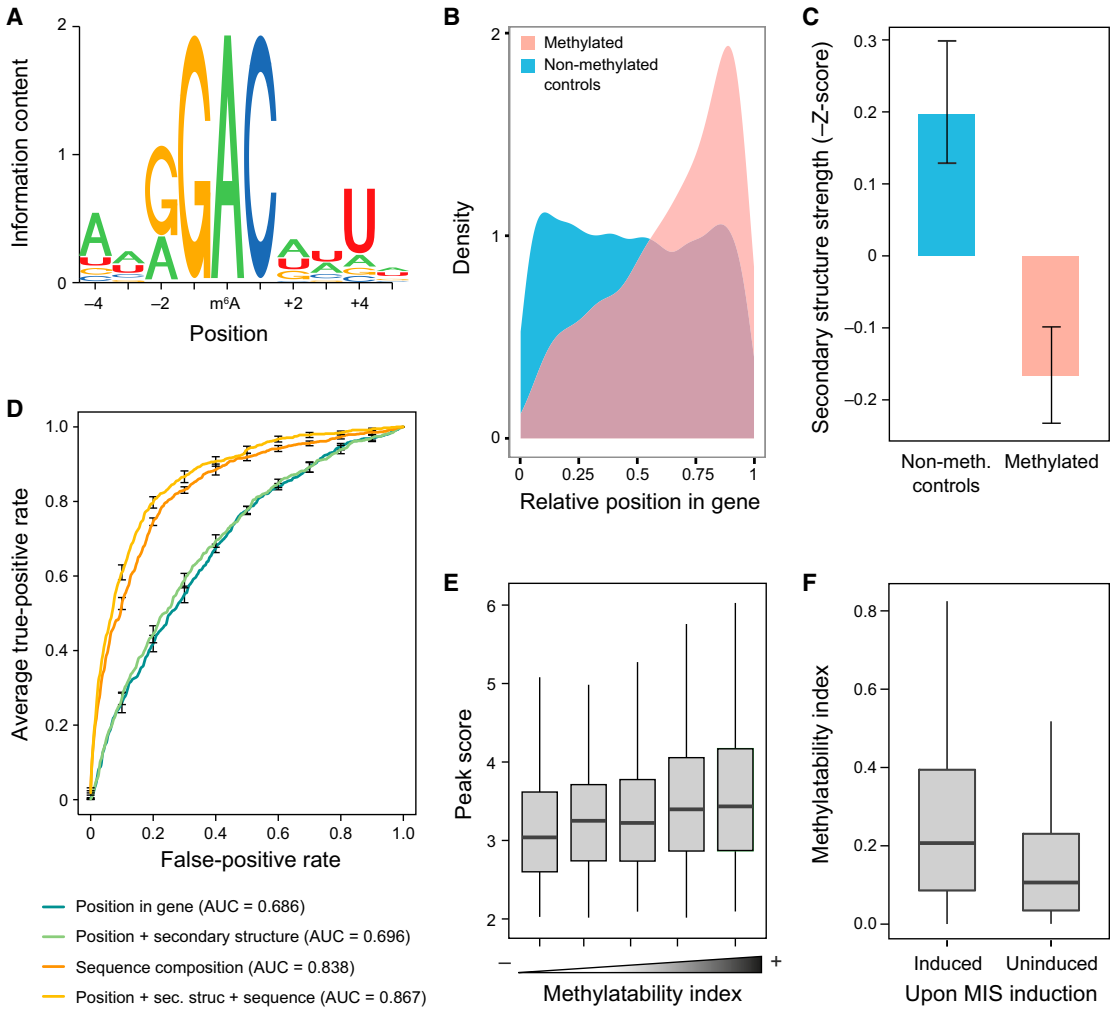

Figure 2. A Methylatability Model Accurately Predicts Methylated Sites Solely from Sequence, Structure, and Relative Position

(A) Methylation motif. Sequence logo of the methylation consensus sequence, based on 711 conservative sites in which the peak was within 5 nt of an RGAC site.

(B) 3′ end bias of methylated. Distributions of the relative position within the transcript (x axis: 0, 5′ end; 1, 3′ end) for methylated sites (pink) and for sites randomly selected within the same genes (blue).

(C) Methylated sites are less structured. Z scores for stability of local secondary structure (y axis) in a 50 nt window surrounding the methylated position (pink, right) and in random controls (blue, left). Z scores calculated as the minimal free energy by RNA fold, normalized against randomly shuffled sequences of the same length and nucleotide composition. Error bars represent SEM.

(D) Methylatability model. Receiver-operator curves (ROC) depicting the performance of different logistic regression classifiers in predicting a site's methylation state based on different sets of features. A model using position, secondary structure, and sequence motif information (orange) performs best, with the sequence motif contributing the most (red).

(E) Methylatability index. Box plots (boxes: lower quartile, median, and upper quartile; whiskers extend to most extreme point no more than 1.5-fold interquartile range) depicting the distributions of the experimentally measured peak score (y axis) as a function of the computationally assigned methylatability index (x axis).

(F) Sites methylated upon MIS activation have higher methylatability indexes. Box plots depicting the distributions of the experimentally measured peak score (y axis) across sites that underwent methylations upon MIS induction (SAy1248, induced) or that failed to become methylated under these conditions (uninduced).

See also Figure S2.

Position +4 was a uridine in 73% of the cases, and position −4 was an adenosine in 63% of the cases (Figure 2A), resulting in a full yeast consensus sequence ANRG-m^{6}A-CNNT. Second, methylated sites were strongly biased toward the 3′ end of transcripts (Figure 2B, Mann-Whitney, $p = 5.9 \times 10^{-51}$), with the 3′ bias increasing with peak strength (Figure S2). Finally, consistent with previous hypotheses from small-scale studies (Bokar, 2005), methylated sites were significantly less structured in comparison to randomly selected counterparts from the same genes (Mann-Whitney, $p = 1.7 \times 10^{-11}$, Figure 2C) or when controlling for 3′ bias of these regions (Mann-Whitney, $p = 1 \times 10^{-9}$), possibly because these are more exposed to the methylation machinery.

Combining these features, we built a high-quality logistic regression classifier to predict methylated sites from these extended sequence, transcript position, and structure features

alone. We trained the classifier to distinguish between a "negative set" of ~10,000 nonmethylated sequences surrounding an RGAC site and a stringent "positive set" of 832 methylated sites centered around an RGAC consensus (Extended Experimental Procedures) and assessed its performance by 10-fold crossvalidation. A classifier using all three feature types performs best (area under the curve [AUC] = 0.87, Figure 2D), with the largest contribution from the extended sequence motif features. There is a positive correlation between the model-assigned probability of methylation ("methylatability index') and the experimental peak score (a feature on which the model was *not* trained; $p = 2.4 \times 10^{-11}$, Figure 2E), suggesting that the model quantitatively recapitulates the same features perceived by the methylating machinery. Furthermore, sites that were not as robustly methylated following ectopic induction of the MIS complex in nonmeiotic cells also had lower methylatability indices (Figure 2F), suggesting that they are poorer substrates for methylation and are more sensitive to the suboptimal vegetative conditions.

Methylation Sites Are Evolutionarily Conserved across Yeast Species at Levels Comparable to Transcription-Factor-Binding Sites

We next evaluated the evolutionary conservation of individual methylation sites. We applied m^{6}A-seq to *Saccharomyces mikatae*, which sporulates efficiently under lab conditions. We generated an *ndt80*Δ/Δ *S. mikatae* strain and a negative control *ndt80*Δ/Δ *ime4*Δ/Δ strain and applied m^{6}A-seq to each strain under meiotic conditions, as well as to a wild-type strain under vegetative growth, as an additional control. Global analysis of methylated sites revealed very similar patterns to those observed in *S. cerevisiae*, with both MIS-dependent and MIS-independent sites (Figure 3A). The 635 *S. mikatae IME4*-dependent peaks (Table S2) were strongly enriched for a consensus very similar to the *S. cerevisiae* one (Figure 3B), were similarly close to the consensus (median, 4 nt), and had similar 3′ bias (Figure S3).

There is a highly statistically significant overlap in methylated genes between the two species (229/610 methylated genes in *S. mikatae* are also methylated in *S. cerevisiae*; $p = 4.6 \times 10^{-27}$; Figure 3C). This extent of conservation is similar to albeit slightly lower than that previously observed for transcription-factor-binding events (Borneman et al., 2007). In 54 cases, the methylated sites were at precisely orthologous (conserved) positions (e.g., Figures 3D and 3E) and 64 were within a 100 nt window (possibly reflecting positional bias). The remainder were more distant. The extent of conservation was significantly higher than expected by chance (5 and 16, respectively; Experimental Procedures) and increased with 3′ proximity (Figure 3F) and peak strength (Figure 3G), suggesting that conserved sites are more likely to be functional. Thus, our results suggest that mRNA methylation is conserved at the gene level, although there is substantial turnover of both sites and targeted transcripts, consistent with the evolutionary patterns of *cis*-regulatory sequences.

Dynamic Changes in Methylation during Yeast Meiosis

The dynamic nature of methylations in yeast offers a unique opportunity to explore their onset and offset. We measured the RNA methylome with m^{6}A-Seq at six time points along a 3 hr time course from induction of sporulation until meiotic prophase and five time points along a 105 min time course after release from prophase arrest (Figures 4A and 4B).

The temporal methylation profiles were partitioned to three clusters: a "sustained" cluster of sites methylated throughout the time course (26% of sites); a "peaked" cluster of sites methylated only during a narrow time window in meiosis prophase (43%); and an "intermediate" cluster of sites methylated during a broader window (31%). The extent of the methylated window correlated with the peak score (Figure 4C), the methylatability index (Figures 4D and 4E), the presence of an "A" at position −4 of the consensus ($p = 0.03$; Figure S4A), 3′ bias of the site ($p = 5.4 \times 10^{-68}$, Figure S4B), and the extent of conserved methylation in *S. mikatae* ($p = 2.6 \times 10^{-5}$, Figure 4F). Thus, a site's methylatability index and its conservation may reflect both the extent of methylation and its temporal span.

Methylation scores peaked at meiotic prophase across all clusters (Figures 4A and 4G), with onset correlating with increased accumulation of all MIS complex components (Figures 4F and S4C) but offset correlating only with decreased expression of *IME4* (Figures 4G and S4C). Collectively, these results suggest a model in which the methylation profiles across yeast meiosis are determined locally ("in *cis*") via the inherent methylatability of the transcript and globally ("in *trans*") via the interplay of different components of the methylation machinery.

m^{6}A Methylation Is Induced by *IME1*-Mediated Induction of Slz1

To dissect the global regulation imposed on the meiotic methylation machinery, we examined the role of *IME1*, the master regulator of meiosis in yeast. We found that *IME1* is required for mRNA methylation by the MIS complex in the meiotic cell cycle. Diploid cells lacking *IME1* (*ime1*Δ/Δ) failed to accumulate m^{6}A-mRNA during meiosis (Figure 5A). This was not merely due to defects in progression through the meiotic cell cycle, as deletion of *IME2*, which arrests cells at the same point as *ime1*Δ/Δ, did not affect m^{6}A-mRNA levels.

The mRNA methylation defect of *ime1*Δ/Δ strains likely results from a failure to express *SLZ1*, a MIS complex component. First, in an *ime1*Δ/Δ mutant, *SLZ1* transcription is less than 5% of that of wild-type (Figure 5B), whereas that of the other MIS components, *IME4* and *MUM2*, is less substantially reduced. The previously characterized dependence of *SLZ1* activation on Ume6 (the DNA-binding component of the Ime1 transcriptional activation complex) and the presence of a Ume6 DNA-binding motif in the *SLZ1* promoter (Williams et al., 2002) further suggest that Ime1 directly activates *SLZ1* transcription. Second, overexpression of *SLZ1* from the inducible *CUP1* promoter in an *ime1*Δ/Δ mutant restores accumulation of meiotic m^{6}A mRNA, whereas overexpression of either *IME4* or *MUM2* in the *ime1*Δ/Δ mutant cannot bypass the m^{6}A accumulation defect (Figure 5C).

mRNA Methylation Requires Nucleolar Localization of the MIS Complex

To determine the cellular compartment in which m^{6}A methylation occurs, we next used immunofluorescence (IF) of each of the three components of the MIS complex at meiotic prophase,

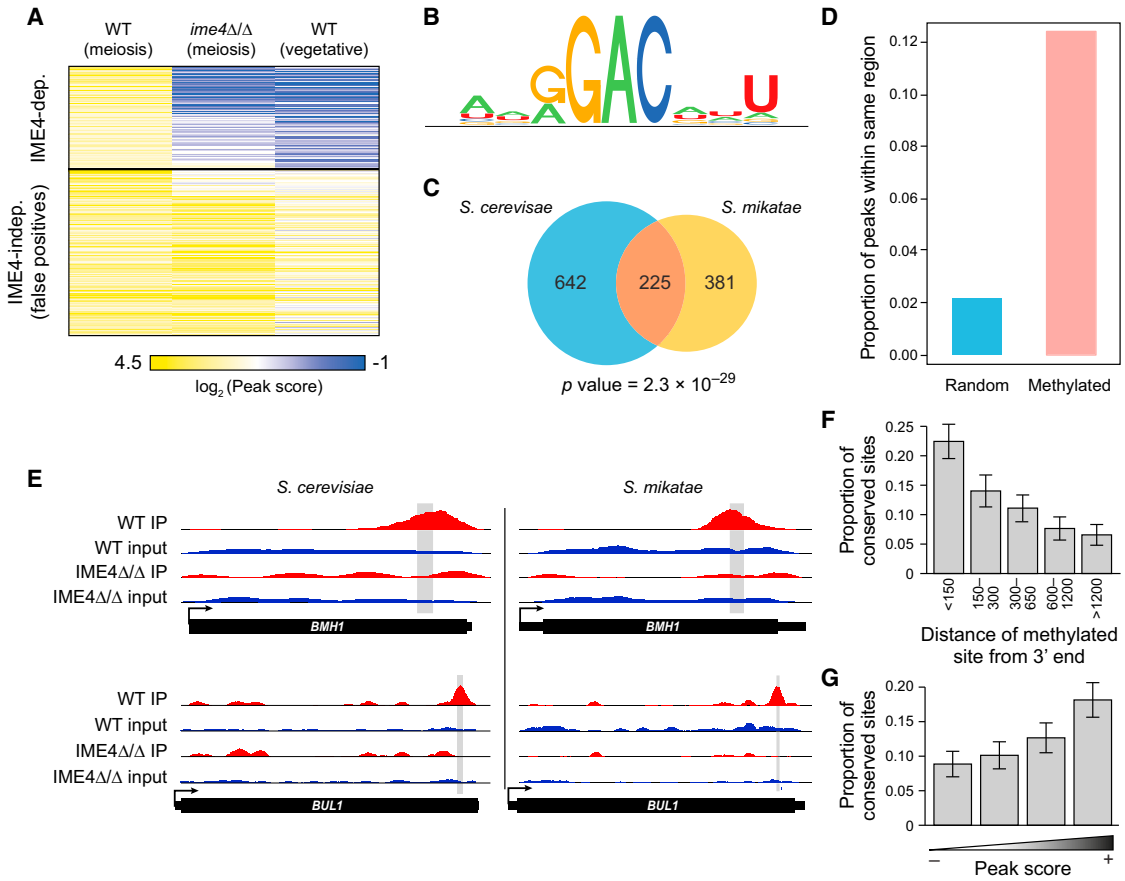

Figure 3. Evolutionary Conservation of Methylation between *S. cerevisiae* and *S. mikatae*

(A) m6A-Seq of *S. mikatae*. Heatmap shows the peak scores (as in Figure 1) for 3,345 peaks (rows) that were enriched (peak score > 2) in *S. mikatae* WT strain under prophase arrest conditions (columns: wild-type meiosis; *ndt80*Δ/Δ, SAy1428; *ime4*Δ/Δ *ndt80*Δ/Δ, SAy1429; wild-type vegetative, SAy1426). Sites are clustered using k-means clustering. MIS-dependent (top) and -independent (bottom) sites are denoted.

(B) *S. mikatate* methylation consensus motif.

(C) Significant conservation of methylated genes. Venn diagram depicting the overlap between genes methylated in *S. cerevisiae* (blue), *S. mikatae* (orange), and both (pink) and the associated hypergeometric p value.

(D) Significant conservation of methylated sites. The proportion of sites detected in *S. cerevisiae* that are also detected within the orthologous 100 nt region in *S. mikatae* (pink bar). (Blue bar) Proportions for a random set of controls.

(E) m^{6}A-seq profiles for two example meiosis genes (methylated near their 3′ terminus) with orthologous methylated positions.

(F and G) Stronger and more 3′ sites are more conserved. Proportion of conserved sites (y axis) as a function of distance from the 3′ end of the transcript (F) or of peak score in *S. cerevisiae* (G). Error bars represent SEM.

See also Figure S3 and Table S2.

when m^{6}A-mRNA levels are maximal. IF of nuclear spreads showed that MIS components were largely excluded from the meiotic chromosomes but were concentrated in a small compartment of the chromosomes that costained with Fob1, a marker of the nucleolus (Figure 5D). In addition, whole-cell IF revealed that these components are also found in the cytoplasm (Figure S5A).

Localization of the MIS complex along a sporulation time course (Figure 5E) shows that the complex localizes to the nucleolus only during the induction of m^{6}A mRNA methylation; nucleolar colocalization is subsequently lost at later phases, corresponding to return to basal levels of m^{6}A mRNA. Both Mum2 and Ime4 colocalized with the nucleolus during the period of m^{6}A mRNA accumulation (between premeiotic S phase and induction of the meiotic divisions MI and MII, ~3 hr in SPO medium) (Agarwala et al., 2012), after *IME1* induction and before *NDT80* induction (Figure S5B). Conversely, as m^{6}A mRNA levels returned to basal levels upon *NDT80* induction and the meiotic divisions (Figure 5E, S9B, 4–7 hr in SPO), Ime4 and Mum2 lost their nucleolar colocalization (Figure 5E), though both remained in cytoplasmic puncta throughout the meiotic time course (Figure S5C).

Loss of nucleolar localization and offset of m^{6}A methylation in later phases of meiosis (Figure 5E) depend on Ndt80 activation. Cells that do not express *NDT80* at the end of meiotic prophase retain high levels of m^{6}A mRNA (Agarwala et al., 2012) and nucleolar colocalization of both Ime4 and Mum2 (Figure 5F). Induction of *NDT80* at this time point, however, leads to the

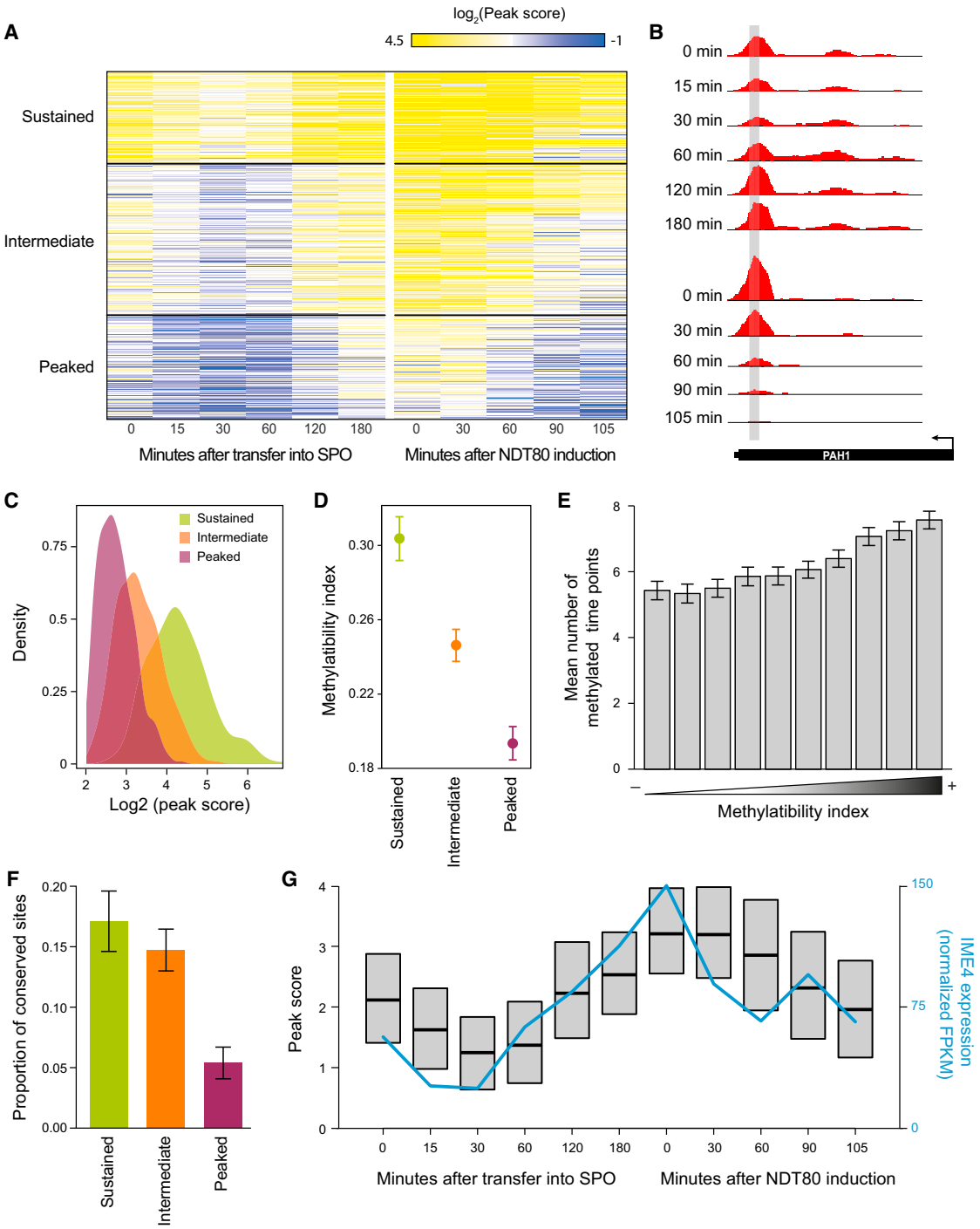

Figure 4. Dynamic Changes in Methylation across Meiosis Reflect Inherent Methylatability

(A) Sustained, intermediate, and peaked methylation profiles across a meiosis time course. Peak scores (as in Figure 1) for 1,308 peaks (rows) at six time points up to prophase arrest and five time points following *NDT80* induction and release from arrest (SAy995) (columns). Sites clustered using k means.

(B) m^6A-seq at the "sustained" site in the *PAH1* transcript.

(C) The temporal window of methylation is consistent with the peak score. Density plots of the distributions of peak score at prophase arrest (Figure 1A) in the sustained (green), intermediate (orange), and peaked (purple) clusters.

(D and E) The temporal window of methylation is longer for genes with higher methylatability index.

(D) Mean methylatability index (y axis; error bars represent SEM) for transcripts in the sustained (green), intermediate (orange), and peaked (purple) clusters.

(E) Bar plots of the average span of methylations (number of time points throughout methylation in which peak scores were greater than 2) at 10 quantiles of methylatability index (x axis). Error bars represent SEM.

(legend continued on next page)

downregulation of mRNA methylation (Agarwala et al., 2012) and loss of the nucleolar localization of Ime4 and Mum2 (Figure 5F).

Nucleolar Entry of the MIS Complex Is Mediated by Slz1

MIS complex entry to the nucleolus is regulated by Slz1 and is necessary for full levels of m^{6}A mRNA accumulation in meiosis. Sequence analysis indicates that Slz1, but neither Mum2 nor Ime4 has a nuclear localization signal (NLS) peptide encoded in its N terminus (Figure 5G). Neither Ime4 nor Mum2 localize to the nucleolus during meiosis in the *ime1*Δ/Δ strain, in which Slz1 is not expressed and there is a defect in mRNA methylation. Expression of Slz1 in this strain restored mRNA methylation and nucleolar localization of both proteins (Figure 5H). Expression of a *SLZ1* allele lacking its NLS failed to overcome the m^{6}A defect. However, replacing the NLS with the SV40 NLS, the noncanonical A1 NLS, or the N-terminal signal sequence of the nucleolar structural protein Nop1 mitigated this defect (Figure 5G). These data suggest that Slz1 is responsible for the nucleolar localization of Ime4 and Mum2 and that this localization is necessary for full levels of m^{6}A mRNA accumulation in meiosis.

Evolutionary Analysis Reveals Coevolving m^{6}A "Writers" and "Readers" from Yeast to Mammals

To identify additional components of the methylation program, we searched for proteins sharing a similar evolutionary trajectory with METTL3, the mammalian ortholog of *IME4*, across 86 eukaryotic species, spanning mammals, other animals, fungi, plants, and protists (Tabach et al., 2013a, 2013b) (Figure 6A). The top 20 coevolving genes included Wilms tumor-1-associated protein (WTAP), the mammalian ortholog of MUM2, and FIP37, a plant ortholog (Zhong et al., 2008), as well as the proteins from the YTH family, two members of which (YTHDF2 and YTHDF3) we have previously found as m^{6}A "readers" that selectively bind m^{6}A in mammals (Dominissini et al., 2012). The yeast homolog identified in this analysis is *ydr374c*, henceforth referred to as *m*ethylated *R*NA-*b*inding protein *1* (*MRB1*).

To validate *MRB1* as an m^{6}A reader, we used affinity chromatography proteomics to identify proteins that selectively bind methylated RNA compared to nonmethylated counterparts. We exposed protein lysate isolated from meiotic yeast cultures to either methylated or nonmethylated baits and analyzed the bound proteins by quantitative mass spectrometry (Experimental Procedures). Strikingly, Mrb1 was the top candidate, showing reproducible preferential association with methylated baits (Figure 6B), and the only one with a >2-fold enrichment in both experiments. *MRB1* is expressed in a meiosis-specific manner, consistent with the meiosis-restricted methylation (Figure 6C), and its deletion led to defects in meiotic progression, albeit less severe than in the *ime4*Δ/Δ strain (Figure S6). These data support a role for Mrb1 as an m^{6}A reader, conserved from yeast to mammals, highlighting the overall conservation of this ancient cellular function.

DISCUSSION

High-Resolution Methylation Maps

We used our dynamic m^{6}A maps during yeast meiosis to identify high-confidence methylated sites at nearly single-nucleotide resolution. We achieved this resolution by optimizing the pull-down protocol and eliminating many false positives with methylation-deficient control strains. This is a substantial improvement over mammalian m^{6}A-seq studies (Dominissini et al., 2012; Meyer et al., 2012) and dramatically expands over the single-methylated site previously validated (Narayan and Rottman, 1988). We found that ~50% of identified peaks are false positives, highlighting the importance of our controls and filtering criteria, using (1) strains/conditions in which methylation is globally absent and (2) in-vitro-transcribed controls. The latter may be particularly useful in mammals, where depletion of the methyltransferase complex leads to apoptosis (Bokar, 2005; Dominissini et al., 2012). Such false positives may impact other nucleotide-affinity assays (e.g., meDIP). Nonetheless, it is possible that our stringent filtering results in false negatives and that some residual false positives remain.

Conservation of Methylation Machinery and Topology

We uncovered several striking similarities between mRNA methylation in yeast and in mammals, suggesting that yeast is a relevant model for m^{6}A methylation. In both yeast and mammals, methylations occur at an RGAC core consensus (Dimock and Stoltzfus, 1977; Dominissini et al., 2012; Meyer et al., 2012; Narayan et al., 1994; Schibler et al., 1977; Wei et al., 1976), albeit with divergence of the broader consensus. Mammalian methylations are highly enriched near stop codons (Dominissini et al., 2012; Meyer et al., 2012), and in yeast, they are 3′ biased and tightly correlated with the stop codon (only 4.7% of the identified peaks occur in the 3′ UTR). m^{6}A writers (mammalian *METTL3/WTAP*, yeast *IME4/MUM2*) and readers (mammalian YTHDFs, yeast MRB1) have coevolved. The YTH RNA-binding domain is present across all eukaryotes (Zhang et al., 2010). Notably, the *Schizosaccharomyces pombe* Mrb1 ortholog, Mmi1p, is essential for eliminating meiosis-specific transcripts during vegetative growth (Harigaya et al., 2006), suggesting a common meiosis-related role of methylation in both species.

A key difference between mammal and yeast is in the dynamic nature of the methylation program. In mammals, methylation profiles are similar across examined conditions and readers and writers are broadly expressed, whereas in yeast, both methylation protein expression and the methylation program are confined to meiosis. Although demethylation is controlled by an active process in human through the RNA demethylases FTO (Jia et al., 2011) and Alkbh5 (Zheng et al., 2013), their orthologs are not detectable in yeast, where methylation offset is coupled to MIS complex downregulation and likely proceeds

(F) Sustained and intermediate methylated sites are more likely to be conserved. Proportion of conserved sites between *S. cerevisiae* and *S. mikatae* (y axis) in each of the three temporal clusters (x axis).

(G) *IME4* expression correlates with average methylation. Box plots of the distributions (interquartile range and medians) of peak scores across the time course and *IME4* expression levels by RNA-seq across the time points.

See also Figure S4.

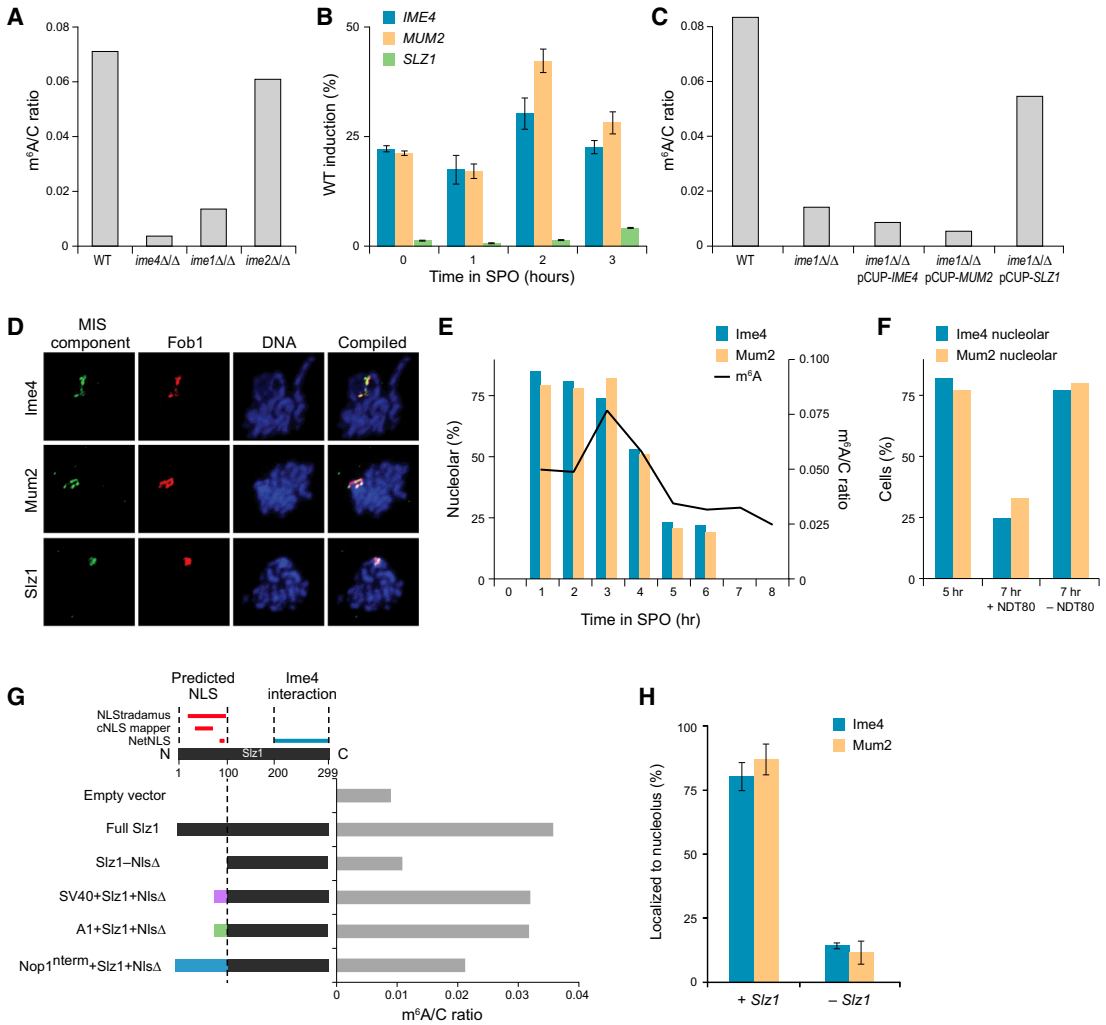

Figure 5. *IME1* Regulates MIS Complex Induction and Nucleolar Localization

(A) Ime1 and Ime4 are essential for m^{6}A methylation in meiosis. TLC-based quantification of mRNA m^{6}A relative to cytosine 3 hr after meiotic starvation, when m^{6}A accumulation is maximal in WT cells (SAy821). m^{6}A levels are reduced in mutants in early meiosis genes *ime1Δ/Δ* (SAy834) and *ime4Δ/Δ* (SAy1196), but not *ime2Δ/Δ* (SAy771).

(B) Ime1 regulates MIS complex gene expression. Induction of *IME4* (blue), *MUM2* (red), and *SLZ1* (green) transcripts in *ime1*Δ/Δ background relative to wild-type (by qPCR). Error bars represent SD of four replicates.

(C) *SLZ1*—but not *IME4* or *MUM2*—overexpression rescues the *ime1Δ/Δ* methylation defect. Quantification of mRNA m^{6}A relative to cytosine 3 hr after meiotic starvation. Wild-type (SAy821) levels are reduced in *ime1Δ/Δ* (SAy834) background. Conditional expression of *IME4* or *MUM2* from the *CUP1* promoter in *ime1Δ/Δ* (SAy1383 and SAy1384, respectively) does not overcome this defect, whereas expression of *SLZ1* does (SAy1385).

(D) The MIS complex localizes to the nucleolus during meiosis. Representative images of immunofluorescence of spread meiotic nuclei, showing colocalization of epitope-tagged Ime4 (SAy914), Mum2 (SAy1235), or Slz1 (SAy1254) (first column) with the nucleolar marker Fob1 (second column). Blue: DNA (DAPI, third column). Compilation (fourth column): DNA, blue; MIS component, green; Fob1, red.

(E) Nucleolar entry and exit of the MIS complex correspond to onset and offset of m6A methylation during meiosis. Quantification of the percentage of cells (y axis) that show nucleolar colocalization of either Ime4 (blue bars) or Mum2 (red bars) upon induction into sporulation medium. Nucleolar colocalization was determined by immunofluorescence of nuclear spreads (n = 100 Fob1 foci/time point); percent colocalization at 7 and 8 hr was not quantified, as the majority of cells were spores at this time point. (Black curve) m^{6}A abundance relative to cytosine throughout meiosis (right axis). All data were collected from a single meiosis in strain SAy1232.

(F) Nucleolar exit dependent on NDT80. Percentage of cells showing nucleolar colocalization of Ime4 (blue bars) and Mum2 (orange bars) after treatment with 1 μM estradiol (+NDT80) or with solvent (−NDT80) (strain SAy1469). Cells were treated at 5 hr and were assayed for nucleolar colocalization after 2 hr of development in the respective medium. Nucleolar colocalization was determined by immunofluorescence of nuclear spreads (n = 100 Fob1 foci/time point).

(G) (Top) Schematic of domains of Slz1, showing predicted nucleolar localization sequence. (Bottom) Levels of m^{6}A normalized by cytosine (x axis, blue bars) in IME1 deletion strains with either an empty expression vector (empty plasmid, SAy1432) or various alleles of SLZ1 (SAy1422, 1434, 1438, 1441, and 1439, respectively). Samples were taken 3 hr after strains were induced into meiosis.

(H) Quantification of nucleolar colocalization events of either epitope-tagged Mum2 (orange) or Ime4 (blue) with Fob1 in an *ime1Δ/Δ* P_{CUP1}-*SLZ1* strain (SAy1385) with either induction (+*SLZ1*, left) or no induction (−*SLZ1*, right). Error bars represent SD of three time points during meiotic prophase. n = 100 cells per time point. See also Figure S5.

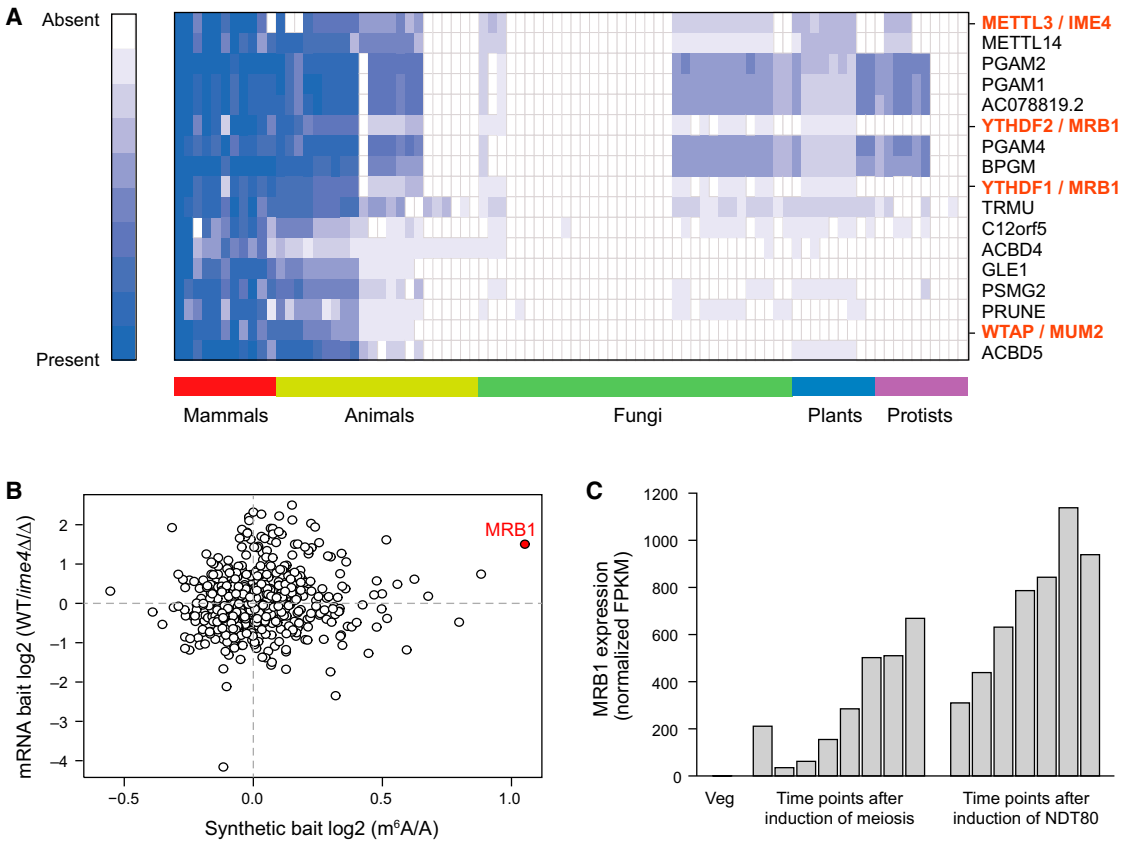

Figure 6. Coevolution of m^{6}A "Writers" and "Readers" across Eukaryotes

(A) Coevolution of m^{6}A readers and writers. Phylogenetic profiles for the top 20 proteins coevolving with human METTL3 across 85 other eukaryotic genomes. For each query protein, the normalized ratio of the BLAST score for the top-scoring protein sequence similarity is indicated in the cell corresponding to each genome. (White) 0, no similarity; (blue) 1, 100% similarity.

(B) MRB1 binds methylated RNA. Mass-spectrometry-based quantification of the levels of proteins pulled down using methylated and nonmethylated RNA baits (x axis, in vitro transcribed; y axis, poly(A) selected RNA from WT or IME4Δ/Δ strains). (Red) MRB1.

(C) MRB1 expression is induced during meiosis. RNA-seq-derived expression levels (TMM-normalized FPKM values) of MRB1 across a meiotic time course. See also Figure S6 and Table S3.

passively through RNA degradation. Indeed, a longer temporal span of methylation (sustained, intermediate, or peaked; Figure 4) is associated, on average, with longer half-lives (under vegetative conditions [Miller et al., 2011]), supporting a passive model (Figure S7A). However, as degradation may both affect and be affected by methylations fully resolving this interplay will require quantitative monitoring and formal modeling.

cis and *trans* Regulation of Methylation

The extent and temporal span of methylations are explained via a combination of *cis* and *trans* elements. At the *cis* level, the extended sequence motif, 3′-position, and lack local secondary structure all increase methylation level and span, with the latter two helping explain why only 1 in ~40 RGAC sites and only 1 in 10 extended ANNRGACNNT sites are methylated (Extended Experimental Procedures). The lack of secondary structure is consistent with findings that duplex RNA structures are incapable of m^{6}A methylation (Narayan et al., 1994), possibly because structured sites are inaccessible to the MIS complex. A yeast cell may use differential methylation in a temporally ordered way across transcripts, analogous to ordered temporal regulation across a regulon (Kalir et al., 2001).

At the *trans* level, the global methylation peak at meiotic prophase is regulated by *IME1* (onset) and *NDT80* (offset). Onset is mediated by Ime1-dependent induction of *SLZ1*, leading to nucleolar localization of the complex. Notably, *IME4* is necessary for *IME1* accumulation (Shah and Clancy, 1992; Hongay et al., 2006; van Werven et al., 2012), and we find that MIS complex activity is necessary for full *IME1* induction (Figures S7B–S7D), suggesting a putative positive feedback loop between RNA methylation and *IME1* expression (Figure 7B). Offset of the methylation program is triggered by *NDT80* induction, leading to exit of the MIS complex from the nucleolus, downregulation of IME4, and termination of the methylation program.

Nucleolar Localization of the MIS Complex

Although the nucleolus is primarily associated with ribosome biogenesis, recent studies have implicated it in mitosis regulation (reviewed in Boisvert et al., 2007). Intriguingly, Misu/Nsun2, an m5C RNA methyltransferase of both tRNA and

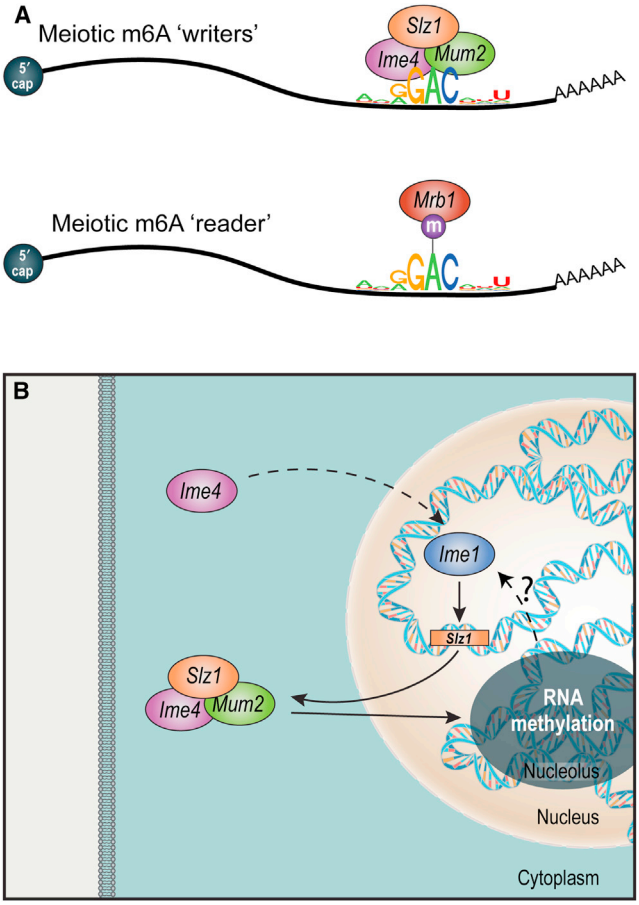

Figure 7. Key Elements in the Yeast Meiotic Methylation Program

(A) The core methylation machinery. The MIS complex (top), active during meiotic prophase, methylates within a sequence motif that is typically 3′ biased and unstructured. The "reader" MRB1 (bottom) binds the methylated motif.

(B) Meiotic regulation of mRNA methylation. IME4 induction leads to IME1 accumulation, which induces SLZ1 expression. SLZ1 forms the MIS complex with MUM2 and IME4 and shuttles them into the nucleolus, where mRNA methylation occurs. mRNA methylation may be required for IME1 activation (dashed arrow marked with a "?"), thereby possibly closing a positive feedback loop.

See also Figure S7.

mRNA (Hussain et al., 2013; Khoddami and Cairns, 2013; Squires et al., 2012), localizes to the nucleolus during interphase (Hussain et al., 2009). Thus, nucleolar localization of the MIS complex raises speculations about nucleolar regulation of both m^5C and m^6A RNA methyltransferases in mitosis and meiosis, as well as the possibility of coordination between mRNA methylation and ribosome biogenesis (we found no evidence for methylated rRNA in our data; data not shown). Notably, mammalian RNA methylation and demethylation occur at nuclear speckles (Bokar et al., 1997; Zheng et al., 2013), which do not appear to have a parallel in yeast (Potashkin et al., 1990).

Possible Functions of Methylation

IME4 deletion delays meiotic progression, as reflected by delays in the induction of *NDT80* and of the two meiotic divisions (Agarwala et al., 2012), and by earlier delays in the formation of the synaptonemal complex and double-strand breaks (Figures S7E–S7G). However, the molecular function of m^6A methylation remains unknown. We observed only modest changes (up to 40% difference) in steady-state expression levels in five of the eight strains in which we eliminated methylation by point mutating the consensus sequence. Three genes had increased levels of expression, and two had decreased (Figure S7H). Furthermore, we observed only a minor global effect of methylations on transcript stability in WT compared to *ime4*Δ/Δ strains, based on monitoring of expression levels across a time course following transcriptional shutoff via thiolutin (data not shown). Our high-resolution yeast methylome and the yeast's tractability will help to test further hypotheses on methylation's role in mRNA processing, export, localization, or translation.

Conclusions

The induction of the MIS complex during meiosis, the regulated temporal dynamics of the methylations, and the impaired progression through meiosis of the *IME4* catalytic mutant strain all strongly suggest that m^6A methylation plays a critical role in yeast meiosis. The striking similarities in methylation profiles and components between yeast and mammals suggest that yeast is a compelling model system for studying the role of methylations. Our high-resolution dynamic maps will pave the way to a better understanding of the roles of RNA methylation and to advance this rapidly emerging field coined RNA epitranscriptomics (Saletore et al., 2012).

EXPERIMENTAL PROCEDURES

See Extended Experimental Procedures for full details.

m^6A-Seq and Analysis

Meiosis was induced and mRNA extracted as detailed in Agarwala et al. (2012). The m^6A pull-down procedure and library preparation is described in the Extended Experimental Procedures. We used a modified version of the approach described in Dominissini et al. (2012) for aligning reads and detecting putative methylated sites based on (1) enrichment at a certain region within a gene compared to background region and (2) absence of this enrichment in the input sample. This pipeline was extended to allow comparison of called peaks across multiple samples/conditions, based on overlapping genomic coordinates. De novo motif analysis and secondary structure analysis was performed as described in Dominissini et al. (2012).

In Vitro Transcription of *IME4*-Independent Peaks

150 nt long DNA templates tiling across 17 genes containing *IME4*-independent peaks were synthesized on a CustomArray 12K Microarray using a B3 Synthesizer (CustomArray, Bothell, WA) and were subjected to in vitro transcription.

Methylation Classifier

A logistic regression classifier was trained to discriminate between a set of RGAC sites and nonmethylated RGAC counterparts. Features used were relative position within the gene, nucleotide composition of positions −4 to +5 with respect to the methylated position, and predicted secondary structure strength. A 10-fold crossvalidation scheme was designed and implemented using the RWeka package (Hornik et al., 2009) in R.

RNA Affinity Chromatography and Mass Spectrometry

Three RNA baits, each comprising a ~120 nt long sequence containing only a single adenine, were in vitro transcribed from dsDNA templates in the

presence of either ATP or N^6-methyl-ATP. These were exposed to proteins isolated from meiotic cultures in prophase arrest. Isolated proteins were labeled via iTRAQ and were subjected to mass spectrometry as described in (Mertins et al. (2013).

Additional Methods

Spread meiotic nuclei were prepared using the method described in Falk et al. (2010). TLC analysis was carried out as in Zhong et al. (2008); mRNA was purified with the Dynabeads mRNA purification system (Invitrogen) and analyzed on cellulose plates (20 × 20 cm) from EMD.

ACCESSION NUMBERS

Sequencing data have been deposited into the Gene Expression Omnibus (GEO; accession number GSE51583).

SUPPLEMENTAL INFORMATION

Supplemental Information includes Extended Experimental Procedures, seven figures, and seven tables and can be found with this article online at http://dx.doi.org/10.1016/j.cell.2013.10.047.

ACKNOWLEDGMENTS

The authors would like to thank Lindsey Dollard and Anna Symbor-Nagrabska for expert technical assistance; Hannah Blitzblau, Mitchell Guttman, and Dmitry Ter-Ovanesyan for fruitful discussions and technical advice; and Leslie Gaffney for making the figures beautiful. The anti-Fob1 antibody was kindly provided by Dr. Stephen Bell. G.R.F. is an American Cancer Society Professor of Genetics. This work was supported by National Institutes of Health Grants GM035010 (G.R.F) and U54 HG003067 (E.S.L.) and Broad Institute Funds. A.R. was supported by an NHGRI Pioneer Award and HHMI. S.S. was supported by an HFSP fellowship.

Received: October 10, 2013
Revised: October 22, 2013
Accepted: October 29, 2013
Published: November 21, 2013

REFERENCES

Agarwala, S.D., Blitzblau, H.G., Hochwagen, A., and Fink, G.R. (2012). RNA methylation by the MIS complex regulates a cell fate decision in yeast. PLoS Genet. *8*, e1002732.

Bodi, Z., Button, J.D., Grierson, D., and Fray, R.G. (2010). Yeast targets for mRNA methylation. Nucleic Acids Res. *38*, 5327–5335.

Boisvert, F.M., van Koningsbruggen, S., Navascués, J., and Lamond, A.I. (2007). The multifunctional nucleolus. Nat. Rev. Mol. Cell Biol. *8*, 574–585.

Bokar, J.A. (2005). The biosynthesis and functional roles of methylated nucleosides in eukaryotic mRNA. In Fine-Tuning of RNA Functions by Modification and Editing, H. Grosjean, ed. (New York: Sprinter), pp. 141–177.

Bokar, J.A., Shambaugh, M.E., Polayes, D., Matera, A.G., and Rottman, F.M. (1997). Purification and cDNA cloning of the AdoMet-binding subunit of the human mRNA (N6-adenosine)-methyltransferase. RNA *3*, 1233–1247.

Borneman, A.R., Gianoulis, T.A., Zhang, Z.D., Yu, H., Rozowsky, J., Seringhaus, M.R., Wang, L.Y., Gerstein, M., and Snyder, M. (2007). Divergence of transcription factor binding sites across related yeast species. Science *317*, 815–819.

Bringmann, P., and Lührmann, R. (1987). Antibodies specific for N6-methyladenosine react with intact snRNPs U2 and U4/U6. FEBS Lett. *213*, 309–315.

Clancy, M.J., Shambaugh, M.E., Timpte, C.S., and Bokar, J.A. (2002). Induction of sporulation in Saccharomyces cerevisiae leads to the formation of N6-methyladenosine in mRNA: a potential mechanism for the activity of the IME4 gene. Nucleic Acids Res. *30*, 4509–4518.

Desrosiers, R.C., Friderici, K.H., and Rottman, F.M. (1975). Characterization of Novikoff hepatoma mRNA methylation and heterogeneity in the methylated 5′ terminus. Biochemistry *14*, 4367–4374.

Dimock, K., and Stoltzfus, C.M. (1977). Sequence specificity of internal methylation in B77 avian sarcoma virus RNA subunits. Biochemistry *16*, 471–478.

Dominissini, D., Moshitch-Moshkovitz, S., Schwartz, S., Salmon-Divon, M., Ungar, L., Osenberg, S., Cesarkas, K., Jacob-Hirsch, J., Amariglio, N., Kupiec, M., et al. (2012). Topology of the human and mouse m6A RNA methylomes revealed by m6A-seq. Nature *485*, 201–206.

Dominissini, D., Moshitch-Moshkovitz, S., Salmon-Divon, M., Amariglio, N., and Rechavi, G. (2013). Transcriptome-wide mapping of N(6)-methyladenosine by m(6)A-seq based on immunocapturing and massively parallel sequencing. Nat. Protoc. *8*, 176–189.

Falk, J.E., Chan, A.C., Hoffmann, E., and Hochwagen, A. (2010). A Mec1- and PP4-dependent checkpoint couples centromere pairing to meiotic recombination. Dev. Cell *19*, 599–611.

Harigaya, Y., Tanaka, H., Yamanaka, S., Tanaka, K., Watanabe, Y., Tsutsumi, C., Chikashige, Y., Hiraoka, Y., Yamashita, A., and Yamamoto, M. (2006). Selective elimination of messenger RNA prevents an incidence of untimely meiosis. Nature *442*, 45–50.

Hongay, C.F., and Orr-Weaver, T.L. (2011). Drosophila Inducer of MEiosis 4 (IME4) is required for Notch signaling during oogenesis. Proc. Natl. Acad. Sci. USA *108*, 14855–14860.

Hongay, C.F., Grisafi, P.L., Galitski, T., and Fink, G.R. (2006). Antisense transcription controls cell fate in Saccharomyces cerevisiae. Cell *127*, 735–745.

Hornik, K., Buchta, C., and Zeileis, A. (2009). Open-source machine learning: R Meets Weka. Comput. Stat. *24*, 225–232.

Horowitz, S., Horowitz, A., Nilsen, T.W., Munns, T.W., and Rottman, F.M. (1984). Mapping of N6-methyladenosine residues in bovine prolactin mRNA. Proc. Natl. Acad. Sci. USA *81*, 5667–5671.

Hussain, S., Benavente, S.B., Nascimento, E., Dragoni, I., Kurowski, A., Gillich, A., Humphreys, P., and Frye, M. (2009). The nucleolar RNA methyltransferase Misu (NSun2) is required for mitotic spindle stability. J. Cell Biol. *186*, 27–40.

Hussain, S., Sajini, A.A., Blanco, S., Dietmann, S., Lombard, P., Sugimoto, Y., Paramor, M., Gleeson, J.G., Odom, D.T., Ule, J., et al. (2013). NSun2-mediated cytosine-5 methylation of vault noncoding RNA determines its processing into regulatory small RNAs. Cell Rep. *4*, 255–261.

Jia, G., Fu, Y., Zhao, X., Dai, Q., Zheng, G., Yang, Y., Yi, C., Lindahl, T., Pan, T., Yang, Y.-G., and He, C. (2011). N6-methyladenosine in nuclear RNA is a major substrate of the obesity-associated FTO. Nat. Chem. Biol. *7*, 885–887.

Kalir, S., McClure, J., Pabbaraju, K., Southward, C., Ronen, M., Leibler, S., Surette, M.G., and Alon, U. (2001). Ordering genes in a flagella pathway by analysis of expression kinetics from living bacteria. Science *292*, 2080–2083.

Khoddami, V., and Cairns, B.R. (2013). Identification of direct targets and modified bases of RNA cytosine methyltransferases. Nat. Biotechnol. *31*, 458–464.

Meyer, K.D., Saletore, Y., Zumbo, P., Elemento, O., Mason, C.E., and Jaffrey, S.R. (2012). Comprehensive analysis of mRNA methylation reveals enrichment in 3′ UTRs and near stop codons. Cell *149*, 1635–1646.

Miller, C., Schwalb, B., Maier, K., Schulz, D., Dümcke, S., Zacher, B., Mayer, A., Sydow, J., Marcinowski, L., Dölken, L., et al. (2011). Dynamic transcriptome analysis measures rates of mRNA synthesis and decay in yeast. Mol. Syst. Biol. *7*, 458.

Narayan, P., and Rottman, F.M. (1988). An in vitro system for accurate methylation of internal adenosine residues in messenger RNA. Science *242*, 1159–1162.

Narayan, P., Ludwiczak, R.L., Goodwin, E.C., and Rottman, F.M. (1994). Context effects on N6-adenosine methylation sites in prolactin mRNA. Nucleic Acids Res. *22*, 419–426.

Potashkin, J.A., Derby, R.J., and Spector, D.L. (1990). Differential distribution of factors involved in pre-mRNA processing in the yeast cell nucleus. Mol. Cell. Biol. *10*, 3524–3534.

Saletore, Y., Meyer, K., Korlach, J., Vilfan, I.D., Jaffrey, S., and Mason, C.E. (2012). The birth of the Epitranscriptome: deciphering the function of RNA modifications. Genome Biol. *13*, 175.

Schibler, U., Kelley, D.E., and Perry, R.P. (1977). Comparison of methylated sequences in messenger RNA and heterogeneous nuclear RNA from mouse L cells. J. Mol. Biol. *115*, 695–714.

Shah, J.C., and Clancy, M.J. (1992). IME4, a gene that mediates MAT and nutritional control of meiosis in Saccharomyces cerevisiae. Mol. Cell. Biol. *12*, 1078–1086.

Squires, J.E., Patel, H.R., Nousch, M., Sibbritt, T., Humphreys, D.T., Parker, B.J., Suter, C.M., and Preiss, T. (2012). Widespread occurrence of 5-methylcytosine in human coding and non-coding RNA. Nucleic Acids Res. *40*, 5023–5033.

Tabach, Y., Billi, A.C., Hayes, G.D., Newman, M.A., Zuk, O., Gabel, H., Kamath, R., Yacoby, K., Chapman, B., Garcia, S.M., et al. (2013a). Identification of small RNA pathway genes using patterns of phylogenetic conservation and divergence. Nature *493*, 694–698.

Tabach, Y., Golan, T., Hernández-Hernández, A., Messer, A.R., Fukuda, T., Kouznetsova, A., Liu, J.G., Lilienthal, I., Levy, C., and Ruvkun, G. (2013b). Human disease locus discovery and mapping to molecular pathways through phylogenetic profiling. Mol. Syst. Biol. *9*, 692.

van Werven, F.J., Neuert, G., Hendrick, N., Lardenois, A., Buratowski, S., van Oudenaarden, A., Primig, M., and Amon, A. (2012). Transcription of two long noncoding RNAs mediates mating-type control of gametogenesis in budding yeast. Cell *150*, 1170–1181.

Wei, C.M., Gershowitz, A., and Moss, B. (1976). 5′-Terminal and internal methylated nucleotide sequences in HeLa cell mRNA. Biochemistry *15*, 397–401.

Williams, R.M., Primig, M., Washburn, B.K., Winzeler, E.A., Bellis, M., Sarrauste de Menthiere, C., Davis, R.W., and Esposito, R.E. (2002). The Ume6 regulon coordinates metabolic and meiotic gene expression in yeast. Proc. Natl. Acad. Sci. USA *99*, 13431–13436.

Zhang, Z., Theler, D., Kaminska, K.H., Hiller, M., de la Grange, P., Pudimat, R., Rafalska, I., Heinrich, B., Bujnicki, J.M., Allain, F.H., and Stamm, S. (2010). The YTH domain is a novel RNA binding domain. J. Biol. Chem. *285*, 14701–14710.

Zheng, G., Dahl, J.A., Niu, Y., Fedorcsak, P., Huang, C.M., Li, C.J., Vågbø, C.B., Shi, Y., Wang, W.L., Song, S.H., et al. (2013). ALKBH5 is a mammalian RNA demethylase that impacts RNA metabolism and mouse fertility. Mol. Cell *49*, 18–29.

Zhong, S., Li, H., Bodi, Z., Button, J., Vespa, L., Herzog, M., and Fray, R.G. (2008). MTA is an Arabidopsis messenger RNA adenosine methylase and interacts with a homolog of a sex-specific splicing factor. Plant Cell *20*, 1278–1288.